# Upscreening of Infineon Hall Effect Sensors for the MMX rover locomotion subsystem

Sedlmayr, Hans-Jürgen und Barthelmes, Stefan und Hacker, Franz und Kunze, Klaus und Maier, Maximilian

The MMX (Martian Moons eXploration mission), conducted by JAXA (Japan Aerospace Exploration Agency) is supposed to explore both Mars moons Phobos and Deimos. This mission is supported by a small rover mutually developed by CNES (Centre national d'etudes spatiales) and DLR (German Aerospace Center), which is intended to land on Phobos. An essential part of that rover is the locomotion subsystem which includes several sensors and eight motors actuating the four legs and the four wheels. In each of the BLDC (Brushless DC) motors are three industrial hall effect sensors mounted which are used for incremental position sensing and motor commutation in parallel. The industrial hall effect sensors TLE 4945L from Infineon were selected instead of space qualified hall effect sensors due to the smaller form factor which is crucial for the rover and the higher accuracy. Since the motors are not located in the warmer inner compartment of the rover, extreme temperatures of -75°C up to +85 °C (non-operational) have to be survived. This temperature range extends the temperature range of industrial electronics and even space grade electronics. Therefore, an up-screening campaign was performed, were the radiation and the temperature performance of the Infineon hall effect sensors were measured. This paper highlights the most important results of the conducted tests.

| Copyright Notice |
| --- |
| ©2022 IEEE. Personal use of this material is permitted. Permission from IEEE must be obtained for all other uses, in any current or future media, including reprinting/republishing this material for advertising or promotional purposes, creating new collective works, for resale or redistribution to servers or lists, or reuse of any copyrighted component of this work in other works. |
| Sedlmayr, Hans-Jürgen und Barthelmes, Stefan und Hacker, Franz und Kunze, Klaus und Maier, Maximilian (2022) Upscreening of Infineon Hall Effect Sensors for the MMX rover locomotion subsystem. In: 2022 RADECS Data Workshop. RADECS Conference, 03.10.2022 - 07.10.2022, Venice, Italy. |

# Upscreening of Infineon Hall Effect Sensors for the MMX rover locomotion subsystem

Hans-Juergen Sedlmayr[1], Stefan Barthelmes[1], Franz Hacker[1], Klaus Kunze[1], and Maximilian Maier[1]

***Abstract*—The MMX (Martian Moons eXploration mission), conducted by JAXA (Japan Aerospace Exploration Agency) aims to explore both Mars moons Phobos and Deimos. This mission is supported by a small rover intended to land on Phobos, jointly developed by CNES (Centre national d'études spatiales) and DLR (German Aerospace Center). An essential part of this rover is the locomotion subsystem, which includes several sensors and eight motors actuating four legs, and the four wheels mount on them.. In each of the BLDC (Brushless DC) motors are three industrial Hall effect sensors mounted, used for incremental position sensing and motor commutation in parallel. Smaller form factor and high accuracy are two key requirements for the selection of the Infinion TLE4945L Hall effect sensors. Since the motors are not located in the insulated inner compartment of the rover, they must withstand extreme temperature ranges of -75°C to +85°C (non operational). This goes beyond the temperature range of industrial electronics and space grade electronics. Therefore, an up-screening campaign was performed, where the radiation and the temperature performance of the Hall effect sensors were measured. This paper highlights the most important results of the conducted tests.**

***Index Terms*—Hall effect sensor, Phobos, Robotic, Rover, Upscreening**

## I. Introduction

The MMX rover, jointly developed by CNES and DLR, shall be deployed on the Martian Moon Phobos. During the mission, the rover aims to explore the surface of Phobos, which is still unknown in detail. The environment on the Martian Moon is challenging, with the expected temperatures of -75°C up to +85 °C (non-operating) at the motors - which are not located in the warmer inner compartment (E-Box) of the rover. During operation, the temperatures are heated up to -30°C as minimum, which is acceptable for space qualified parts, but still challenging for industrial parts. Furthermore, the milli-gravity on this moon - around $0.004 - 0.007\mathrm{m/s}^2$ - and the unknown surface properties make it difficult to develop a locomotion subsystem that ensures a proper movement of the rover on Phobos. More details about the mission and the locomotion subsystem development can be found in [1], [2] and [3]. A simulation view of the MMX rover on the surface of Phobos can be seen in Fig. 1.

The locomotion drive chain utilizes two different commercial off the shelf (COTS) parts for the drive electronics: A brushless direct current (BLDC) motor driver from Texas Instruments (DRV8332, [4]), located in the internal E-Box. The second part is an industrial Hall effect sensor TLE 4945L from Infineon [5]. It is selected instead of space qualified Hall effect sensors (e.g. Optek OMH3075, [6]) for the smaller form factor, and the smaller variance of the turn-on and turn-off induction.

[1]These authors are with the Robotics and Mechatronic Center, DLR, Oberpfaffenhofen, Germany; Contact: hans-juergen.sedlmayr@dlr.de

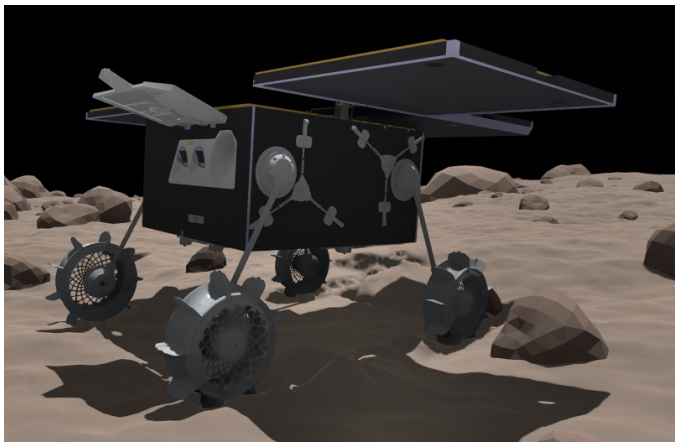

Fig. 1. Simulation view of the full rover in drive configuration. The external shoulder side and the legs with wheels can be seen. Credits: [3], Copyright ©2022, IEEE

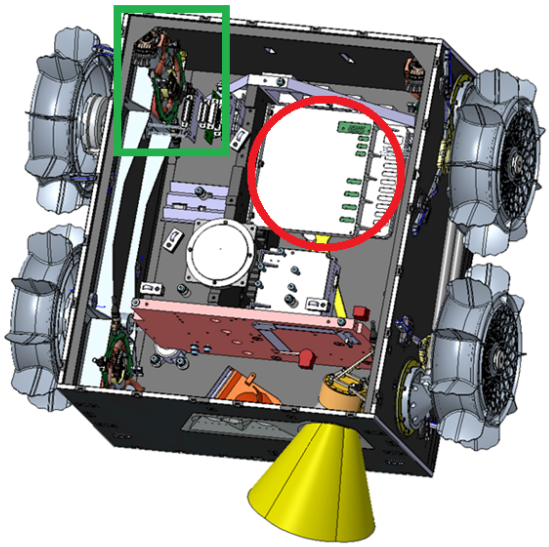

Fig. 2. CAD section drawing of the rover and some of its contents

The reduction of the variance reduces the dependency of the distance between the motor magnets and the Hall effect sensors. Furthermore, it provides improved accuracy of the Hall effect sensor output signal switching edge, which results in an increased efficiency of the motor drive unit.

Fig. 2 shows a CAD section drawing of the rover where the locomotion E-Box (marked with the red circle) and one of the four shoulder modules (marked with the green square). In

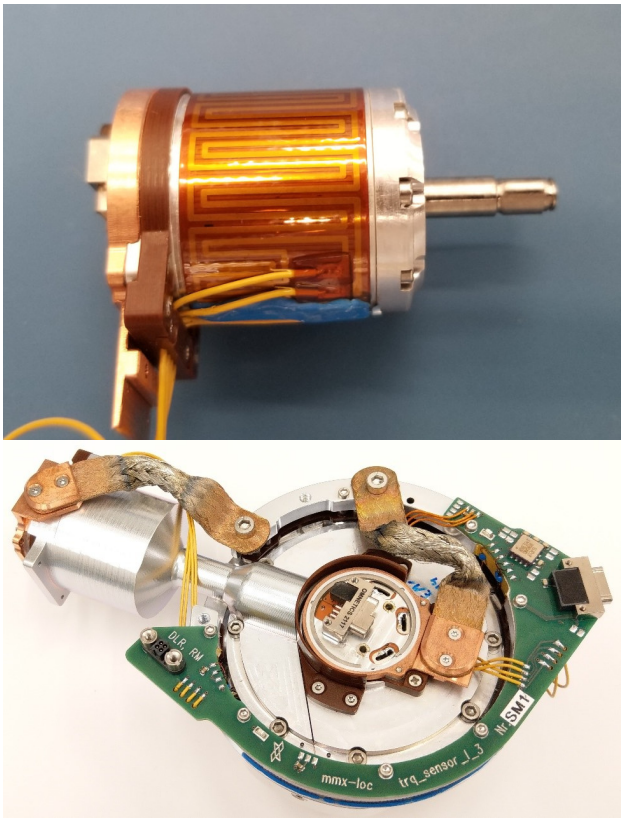


Fig. 3. The actuator (top) and the shoulder module (bottom) - consisting of two actuators, gear boxes and torque sensor Credits: [3], Copyright ©2022, IEEE

each of the eight BLDC motors are three Hall effect sensors mounted which are used for incremental position sensing of the legs and the wheels and for the motor commutation in parallel. The upper sub-figure of Fig. 3 shows an actuator module, while in the lower sub-figure the whole shoulder module is depicted.

The Hall effect sensor family TLE49x5 from Infineon is commercially available for a long time and different models have already been tested several times by multiple companies. Newton et al. evaluated the laser single event effects response of Optek and Infineon Hall effect sensors [7]. Another test was performed in the frame of the ExoMars project [9]. For the BLDC motors of the drilling and sampling mechanism Infineon Hall effect sensors were selected due to the stability against radiation and the huge temperature range by Philips et al. [8].

To the best of our knowledge, a comprehensive test of the Infineon Hall effect sensor TLE4945L is not available, therefore further evaluation of the sensor is required - regardless of the needs for spin-in of COTS parts in space born systems. Similar to the ExoMars project, an up-screening procedure, which includes radiation testing and temperature testing, was necessary for the MMX mission. Within this procedure, the following test campaigns were conducted:

- temperature cycling test with material analysis afterwards
- low temperature operating test
- low TID (Total Ionizing Dose) test with new and temperature cycled parts in parallel
- low proton irradiation test

The following sections summarize the environment and the most important results of this test campaigns. Furthermore a summary of former radiation tests performed with a different lot of the TLE4945L is provided.

## II. Hallsensor TLE4945L

Infineon Technology AG, manufactures the TLE49x5 series of Hall effect sensors ([5]). These sensors were designed for automotive applications with a operating temperature range of -40°C up to +150°C junction temperature. Furthermore, the wide input voltage range from 3.8V to 24V DC in conjunction with a small package PG-SSO-3-2 (Plastic Single Small Outline; through hole; 4.16mm x 3.29mm x 1.52mm) make this part an interesting device for highly integrated motor drive applications.

The open collector output of the bipolar device TLE4945L

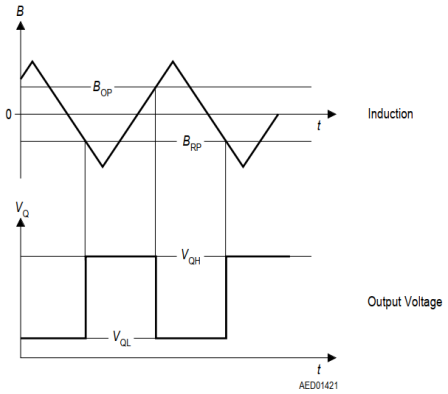


Fig. 4. TLE4945L switching characteristics (TLE49x5L series data sheet) [5]

(Marking on the package is “45L”) will conduct when a positive magnetic field is applied and the magnetic induction is higher than the switching point $B_{OP}$. The output voltage is low during this state. It does not change until a reverse magnetic field is applied where the magnetic induction exceeds the turn-off point $B_{RP}$. More on its operating characteristics is shown in Fig. 4.

The circuit includes the Hall generator, an signal amplifier, and a Schmitt-Trigger with open collector output. Fig. 5 shows the block diagram of the TLE series. The sensors are built in a bipolar Hall switch technology from Infineon with a structural width of $2\mu m$. The IC itself has a size of 1mm x 1mm whereby the Hall generator (quadruple) has a size of $120\mu m$ x $120\mu m$. The bipolar technology employed justifies the need for ELDRS (Enhanced Low Dose Rate Sensitivity) testing.

## III. Environment

According to the mission radiation analysis, all EEE (Electrical, Electronic and Electromechanical) parts outside the internal E-Box must be able to survive a TID (total ionizing dose) exposure of 10 kRad at component level. The spectrum of the Solar heavy ions is depicted in Fig. 6. The calculation of the spectrum included all species from Helium up to Uranium

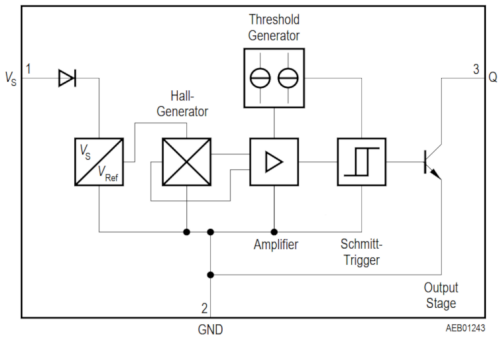


Fig. 5. Block diagram of the TLE4945L (TLE49x5L series data sheet) [5]

during the worst-week-event. The simulation was performed with SPENVIS (SPace ENVironment Information System, [10]). The expected minimum and maximum temperatures for

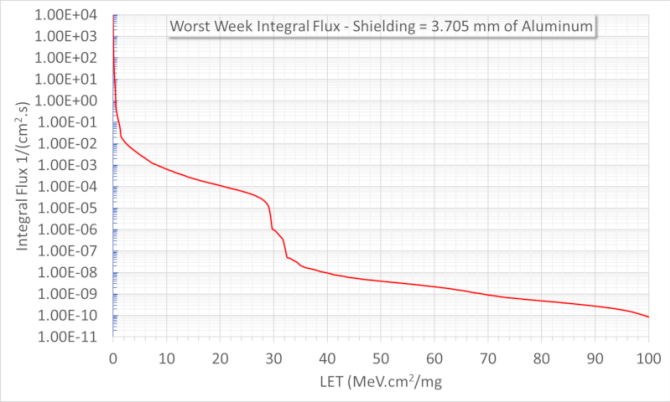


Fig. 6. Solar heavy ions LET spectrum

the locomotion drive units during this mission are -75°C up to +85°C (non-operating) and -30°C up to +85°C (operating). In addition to the extreme temperatures, one Phobos-day lasts only 7 Earth-hours, which means that the resulting thermal gradient is another very challenging topic for the material.

## IV. Thermal Tests

The thermal test campaign consists of two different sub-tests: A thermal cycling test and a low temperature operating test. The first sub-test was conducted at [11] in order to verify the mechanical robustness of the Hall effect sensor device. Fig. 7 shows the fundamental process for the complete test sequence. Initially, samples were collected from a single lot of devices under test (DUT) to suffice the required number of samples. This step is followed by initial inspection to guarantee that none of the samples are impaired or damaged before the cycling itself takes place. The sequence then foresees a full functional test of all samples before and after the cycling to check, that the parts work within their required operational parameters. The cycling procedure consists of 100 cycles between -130°C and +60°C with a dwell time of minimum 15 minutes at the extreme values and a thermal gradient of

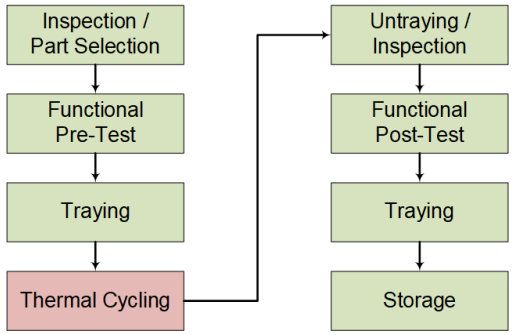


Fig. 7. Basic Test Sequence for the thermal cycling test

at least 1.6°C per minute. Furthermore, the parts are stored in specially designed tray sets that promote the exposure to the cycling environment in order to get most realistic impact on the DUT. After the cycling and testing, the parts are stored for further investigations, e.g. bonding integrity analysis.
The low temperature operating test was conducted in order to determine the behavior and the sensitivity of the Hall effect sensor at deep temperatures, which exceeds the rated temperature range of -40°C up to +150°C. As a second objective, the temperature where the sensors stop their operation should be determined. Fig. 8 shows the temperature profile of the conducted test, where the x-axis shows the elapsed test time. For this test, the same test setup as for the radiation tests was used, which is described in the next chapter. The measured and plotted coil temperature is identically with the Hall effect sensor temperature.

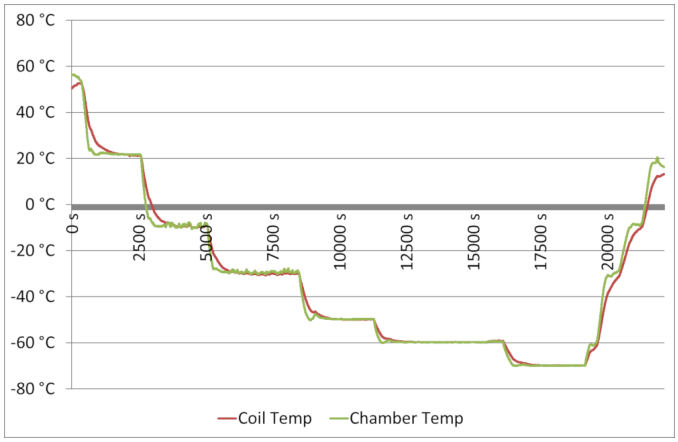


Fig. 8. Thermal Cycling deep temperature functional test, temperature profile

## V. Radiation Tests

This lot acceptance test was conducted in order to review the radiation performance of the Infineon Hall effect sensor. It was conducted with parts in new condition from the lot acquired for the temperature tests, as well as parts already used at the temperature cycling tests in order to identify the difference in the radiation response between the temperature cycled and the non-cycled parts at a Co60 source. Finally, a proton test with both groups was also conducted. Both tests were executed at the Helmholtz Zentrum for Proton Therapy

in Berlin at room temperature [12].
The TID tests were performed in accordance to ESCC 22900 wherever possible at a dose rate of 2,04 Gy/h (low dose rate window, ELDRS testing) until a total dose of 230 Gy(Si) was reached. Due to the Covid pandemic restrictions, the tests were executed remotely, therefore, no annealing measurement was performed after the TID tests.
The proton test was executed in accordance to ESCC 25100 wherever possible with following parameters:

- Flux: $2.0 \cdot 10^7$ Protons / (cm*s)
- Fluence: $2.0 \cdot 10^{10}$ Protons/cm$^2$
- Energies: 68, 50 and 30 MeV/Proton

A test run with heavy ions was omitted due to the Covid pandemic restrictions, as well as the rigorous schedule. This risk was deemed acceptable due to the relaxed environment in conjunction with a very short operating time during this mission.

### A. Test setup

As trigger signal for the Hall effect sensor, a sinusoidal voltage was used, which stimulated a coil. This coil is located close to the DUTs to switch their outputs according to the corresponding magnetic field. Fig. 9 shows the test board with the mounted DUTs on the coil and Fig. 10 the measured B-field of the coil.
The corresponding equation of the used B-field is given in

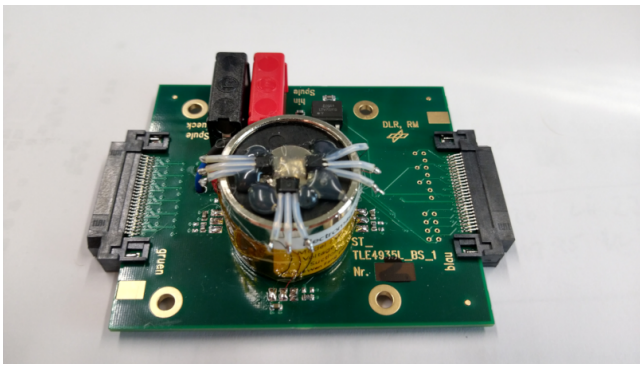

Fig. 9. Test board with the DUTs mounted on the stimulating coil

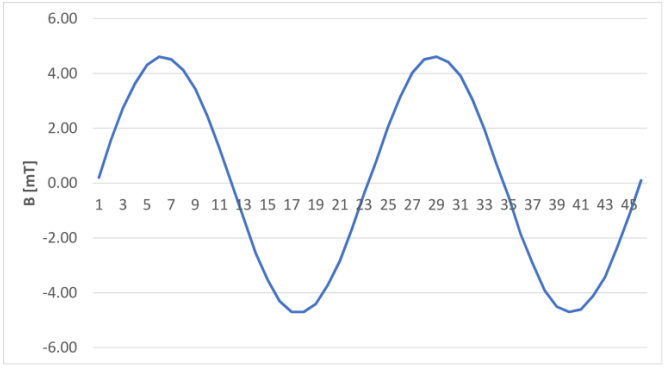


Fig. 10. Measured magnetic field

equation 1. The denominator, which defines the period, is different for the individual test campaigns (between 100 ms and 800 ms), but the amplitude is the same for all tests.

$$b(t) = 4.51mT \cdot \sin(2\pi \cdot \frac{t}{200ms}); \quad (1)$$

Starting at a positive zero crossing of the sinusoidal coil current, the length of $t_{off}$ and $t_{on}$ of the Hall effect sensor output was determined regularly. Fig. 11 shows a graphical overview of the measurement principle, which was used for all test campaigns. Total dose induced effects are based mainly on a shift of the internal threshold generator, which is used to distinguish between the high and low level of the magnetic field. In case of charged particles the physics of the Hall effect itself will be influenced. Therefore, the time between two consecutive edges of the output signal is a good information on the sensors health.
All tests were based on the same testing hardware setup,

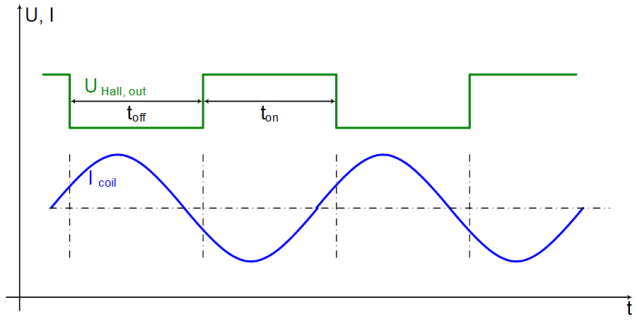


Fig. 11. Hall effect sensor trigger principle

shown in Fig. 12. The radiation test motherboard (RTM) is the central data collecting and test pattern generation unit. On the primary side the RTM provides a RS422 interface to a PC in the control room. The measured data are sent to the PC and all commands for the test execution to the RTM.
The secondary side of the RTM provides up to six variable supply voltages between 3.3V and 6.0V for the DUTs, the trigger signals for the stimulation coils as well as analogue and digital inputs. In case of a latch-up or malfunction, the RTM is able to switch off the power supply of the DUTs and all connected interface circuits in under 5 microseconds, due to the permanent monitoring of the supply voltages. Furthermore, the timing measurement of the Hall effect sensor outputs and the supply current measurement is done by the RTM.
In addition to the RTM, an interface board is needed. This piggyback board contains the +/-30V driver circuitry for the stimulating coil and all connectors to the three DUTs which can be connected to one RTM in parallel. The DUT interface is realized by Samtec ERDC cables. Fig. 13 shows the RTM (lower board) with the mounted interface board (upper board).

### B. TID test results

As already stated, the test campaign was performed with devices in unused condition from the lot and with temperature cycles devices in order to measure differences in the behavior of the devices after the temperature cycling. The test principle,

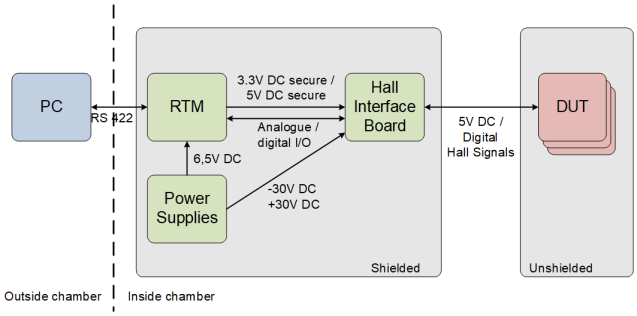


Fig. 12. Hall effect sensor test hardware setup

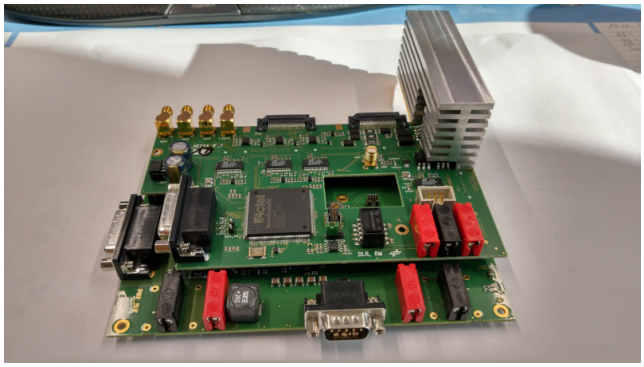

Fig. 13. RTM with mounted interface board

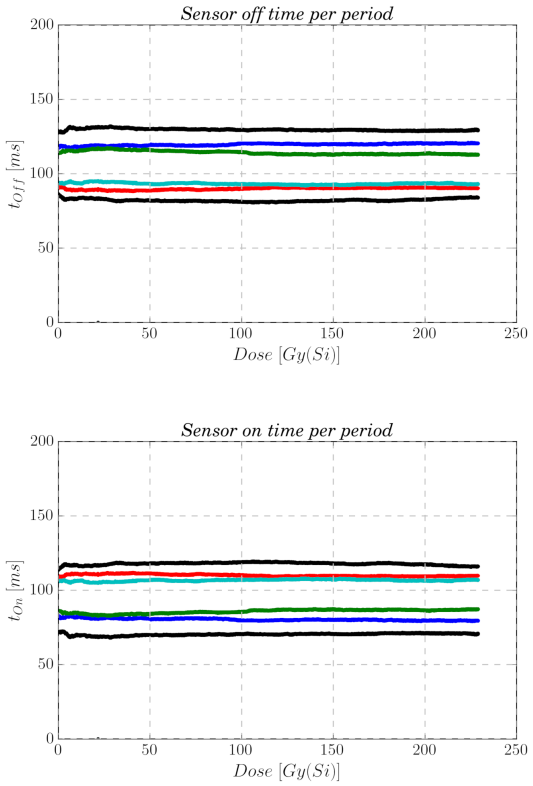


Fig. 14. TID test results of the not cycled devices

shown in Fig. 11, forces a symmetric on and off time distribution of the Hall effect sensor output. But due to uncalibrated positions of the sensors on the coil and inhomogenities of the created magnetic field, the measured output signals are slightly asymmetric. This is not a failure as long as the period is constant or the deviations are within a certain limit.

During the irradiation with a Cobalt-60 source, all important parameter were measured (biased in-situ test at room temperature). The test was performed at a dose rate of 2,04 Gy/h (low dose rate window, ELDRS testing) until a total dose of 230 Gy(Si) was reached.

Fig. 14 shows the measured sensor outputs of 6 different DUTs, which were mounted in two groups of three sensors. Each plotted curve corresponds to one sensor. The group with the longer off-time (upper sub-figure) corresponds to the group with the shorter on-time (lower sub-figure), and vice versa. For this test, the on and off time was set to 100 ms each which result in a period of 200 ms in total.

Fig. 15 shows the results of the thermal cycled and afterwards irradiated DUTs. The period for this campaign was set to 800 ms in order to enlarge the timing resolution. Similar to Fig. 14, two groups of three sensors were irradiated and the group with the longer off-time (upper sub-figure) corresponds to the group with the shorter on-time (lower sub-figure) and vice versa.

Since the differences between both runs are rather small, the average relative deviation D of the measured switching time was calculated according to equation 2.

$$D = \frac{\frac{1}{n}\sum |x - \bar{x}|}{\bar{x}} \tag{2}$$

The results of these calculations are plotted in Fig. 16 for the not cycled devices and in Fig. 17 for the thermal cycled parts. In both figures the deviation of the on-time is plotted in red, while the deviation of the off-time is plotted in blue. Both groups show the same sensitivity against gamma radiation.

The deviation of approx. two percent of the switching time could be transferred in a B-field-deviation as shown in equation 1 for both conducted tests. This leads to a B-field variation of 0.6mT for both tests.

These results have to be reconsidered with respect to the deviation of the sensor sensitivity. According to the data sheet, the Infineon TLE4945L Hall effect sensor has a turn-on induction between -6mT and 10mT, and a turn-off induction between -10mT and 6mT. In total, the hysteresis of the switching threshold is between 2mT and 10mT. Finally, the measured data and the radiation induced error are within the spread for standard factory models.

During the whole test campaign no increase of the supply current was measured for both groups. Therefore, no plot shall be added here.

This is in line with the results of the material inspection (X-Ray inspection, polished micrograph section) which was performed with some devices of the thermal cycled lot. Neither the X-Ray inspection nor the polished micrograph section showed any cracks or damages of the analyzed devices.

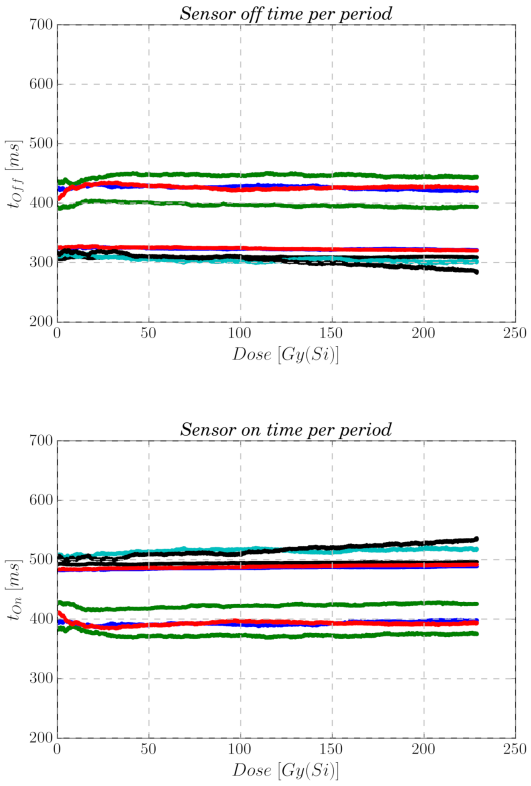


Fig. 15. TID test results of the thermal cycled devices

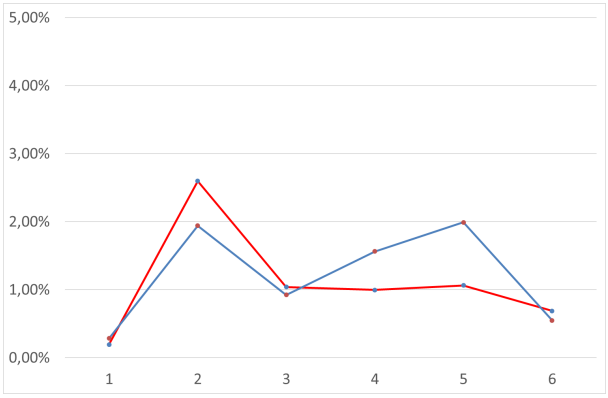


Fig. 16. Deviation of switching time (new devices)

### C. Proton test results

During the proton test campaign no serious error was measured. Similar to the plots in the previous sections, the deviation of the on-time is plotted in red, while the deviation of the off-time is plotted in blue. However, contrary to the dose information, the beam time is used as x-axis. In order to have a compact plot, all test sections with the different particle energies are concatenated. The start of each section is indicated by a colored vertical dotted line. These sections correspond to the proton energies: 68 MeV (I); 50 MeV (II); 30 MeV (III). Fig. 18 and Fig. 19 show the results of the proton test campaign, where each subplot contains data from

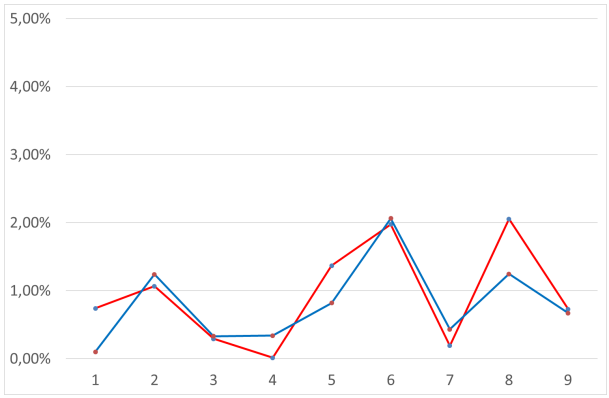


Fig. 17. Deviation of switching time (thermal cycled devices)

the temperature cycled and the not cycled parts.

The first subplot of Fig. 18 shows the sensor off time

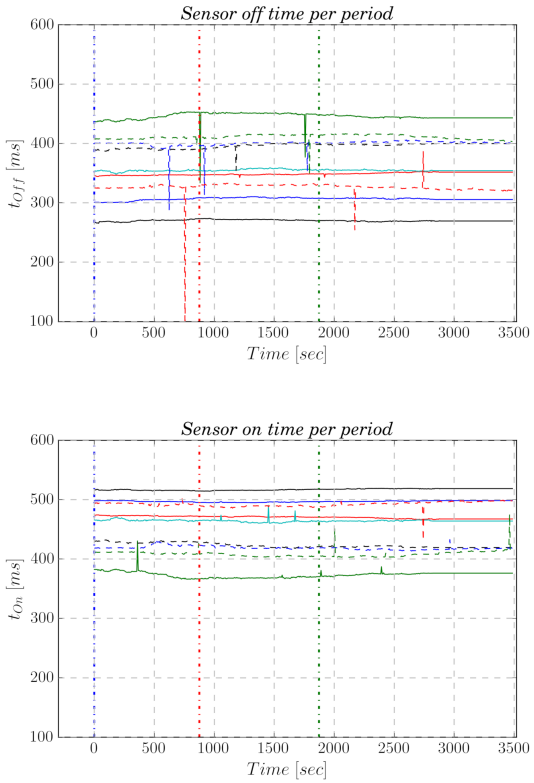


Fig. 18. Proton test results, part I (both groups)

measurements, where the output of the Hall effect sensors was set to logic low state, while the second subplot shows the sensor on time measurements. The first subplot of Fig. 19 contains the sum of both measurements which should be a constant value according to equation 3.

$$t_{sum} = t_{on} + t_{off} = t_{const} \tag{3}$$

A few deviations in the sensors response to the magnetic field based on particle strikes were measured at the sensor output, which appear as upsets in the subplots of Fig. 18 and 19. After

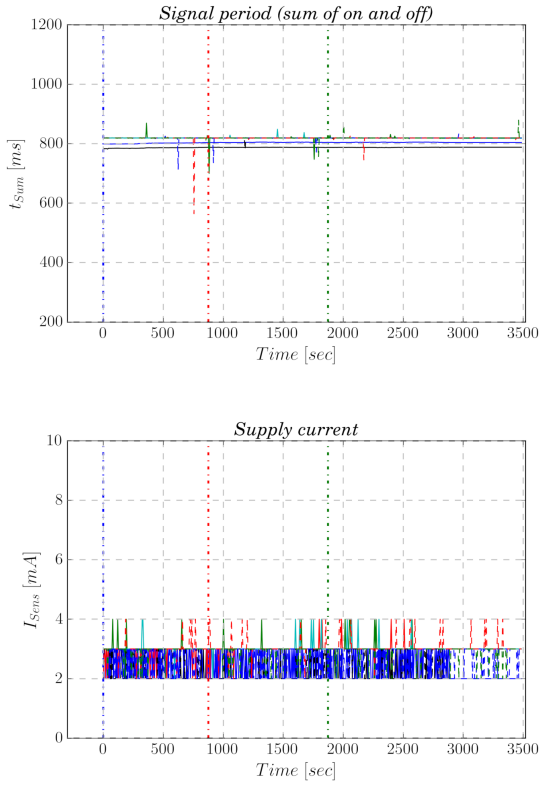


Fig. 19. Proton test results, part II (both groups)

analyzing the data more in detail, no dependency on the status of the sensors (thermal cycled or not) could be determined. These measured deviations lead to a violation of equation 3, since the switching operation is triggered by the protons, and not primarily by the stimulating coil.

Finally, the second subplot of Fig. 19 shows the supply currents of the Hall effect sensors. A few minor upsets were measured during the irradiation with protons, but no single event latch-up (SEL) or other catastrophic event occurred during this test campaign.

During the proton irradiation a total dose of 104.6 Gy(Si) was deposited in the devices (according to the equations which are given in [13]). This is in line with the performed total ionizing dose tests, therefore, no dose based defects of the parts were expected in advance and measured during the irradiation.

## VI. Comparison with former test campaigns

This type of sensors (not the exact same batch from before) were already irradiated in different prior campaigns. This section summarizes the results of these earlier test campaigns and compares the activities.

The test principle was similar for all test campaigns, but the period of the sinusoidal stimulation is different for each test. Especially for the comparison between the cycled and non-cycled devices, the period was enlarged to increase the timing resolution during the measurements for MMX.

Starting with a high dose rate test to find a possible flight candidate, the TID irradiation at room temperature was stopped at a dose level of 1042 Gy(Si) without significant degradation. Fig. 20 shows the sensor on and off time over dose combined in the upper sub-figure and the supply currents over dose in the lower sub-figure. The rated current of the device is according to the data sheet between typical 3 mA and maximal 8 mA. The measured currents are within the expected limits.

The next TID test was performed with low dose rate (3,08

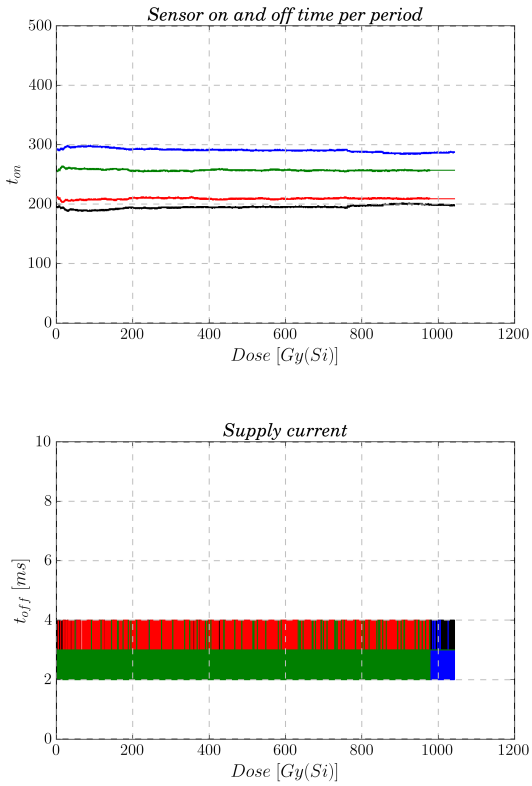


Fig. 20. Test results for high dose rate test, possible flight candidate evaluation

Gy(Si)/hour). The irradiation was conducted until a total dose of 520 Gy(Si) was reached. Then it was stopped due to time constraints but not due to device damages. Fig. 21 shows the results of this test. Similar to the last section the figure is divided in two corresponding to the two different states of the sensor output. Where the output measurement with the longer off period corresponds to the output measurement with the shorter on period and vice versa. During the complete test, no increase of the supply current was measured. Therefore, no figure is added here.

Similar to the results of the MMX test campaign, the TID test results of the flight candidate evaluation, are promising. The measured drift of the switching time is within the tolerance of the switching time caused by the deviation of the sensor sensitivity.

At the RADEF (RADiation Effects Facility, [14]) a heavy ion test campaign was also performed. The test was conducted in vacuum at room temperature with the rated supply voltage. For the irradiation the 9.3 MeV/u cocktail of the test facility was used. All devices were delidded by chemical etching. Table I shows the used ion species, the applied tilt angle and the

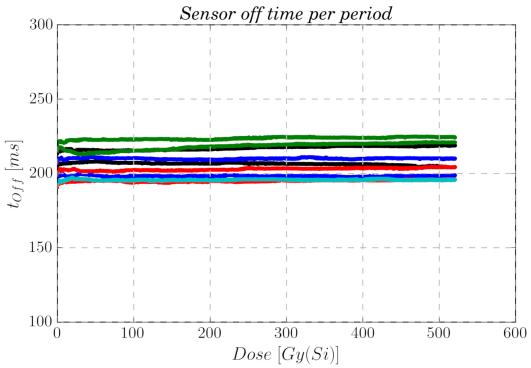


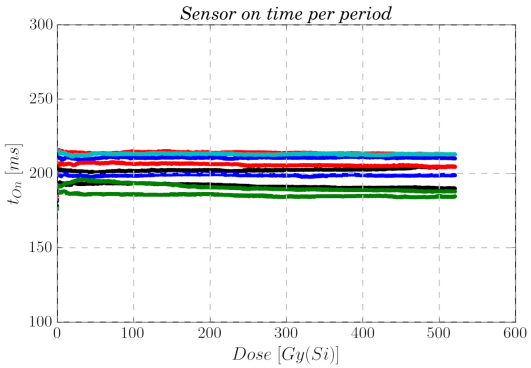


Fig. 21. Test results for low dose rate test, possible flight candidate evaluation

effective LET. A tilt angle of 0 degree is the normal incidence of the beam. The applied fluence of 1.0E+7 ions per square centimeter was used for each ion species.

Fig. 22 shows the first generation of the Hall effect sensor test board mounted in the vacuum chamber at RADEF. The stimulating coil is on the backside of the board. Contrary to the actual version of the test board, shown in Fig. 9, the old one was only able to carry two DUTs marked by red circles.

TABLE I
USED ION SPECIES AND THEIR LET VALUES

| section | ion species | tilt-angle $[degree]$ | effective LET $[MeV \cdot cm^2/mg]$ |
|---|---|---|---|
| 1 | $^{15}N^{4+}$ | 0 | 2.0 |
| 2 | $^{15}N^{4+}$ | 60 | 6.0 |
| 3 | $^{56}Fe^{15+}$ | 0 | 24.5 |
| 4 | $^{56}Fe^{15+}$ | 53 | 40.7 |
| 5 | $^{83}Kr^{22+}$ | 32 | 45.9 |
| 6 | $^{83}Kr^{22+}$ | 45 | 55.1 |
| 7 | $^{131}Xe^{35+}$ | 42 | 92.8 |
| 8 | $^{131}Xe^{35+}$ | 48 | 103.0 |

Fig. 23 shows the results of the heavy ion tests, with the same color code as in the proton test plot, and the beam time is used as the x-axis. In order to have a compact plot, all test sections with the different ion species are concatenated. The start of each section is indicated by a colored vertical dotted line. These sections correspond to the column '*section*' of table I.

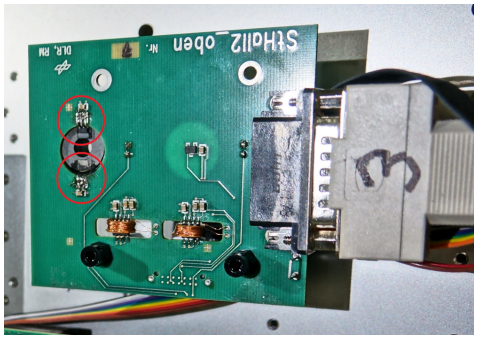


Fig. 22. Testboard (first generation) with DUTs in the vacuum chamber

Until the end of the test no SEL, other high current events or SEFI (single event functional interrupt) were measured. But obviously the sensor output is rather noisy. The nominal sensor on/off time without irradiation was 250 ms for this campaign. But due to irradiation with the heavy ions, the output switches rather irregular, but is still triggered by the stimulating coil.

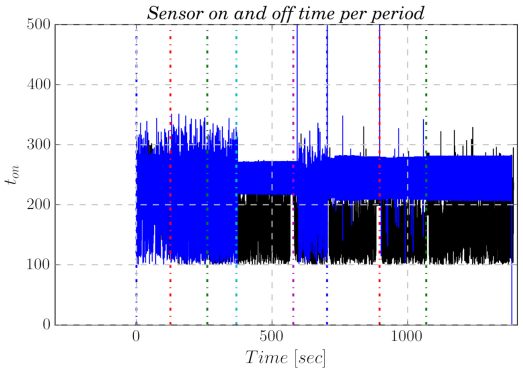


Fig. 23. Test results heavy ion test, possible flight candidate evaluation

A reason for this is the nature of the Hall effect itself which relays on the generation of a voltage difference (the Hall voltage) across an electrical conductor when a magnetic field is applied perpendicular to the voltage. [16] describes the Hall effect more in detail, and Fig. 24 shows an artists view of the Hall effect.

The Hall voltage can be calculated according to equation 4 ([15]), where is *I* the current through the Hall element, *B* the magnetic flux density, *d* the thickness of the conductor, *n* the charge carrier density (material constant) and *e* the charge of each carrier in the conductor.

$$U_{Hall} = \frac{1}{n \cdot e} \frac{I \cdot B}{d} \tag{4}$$

During the irradiation with charged particles, the equilibrium of the electric forces on the charge carriers is disturbed which results in higher or smaller Hall voltages. This triggers the output of the Hall effect sensor in an uncontrolled manner, which is clearly visible in Fig. 23. This effect is also mea-

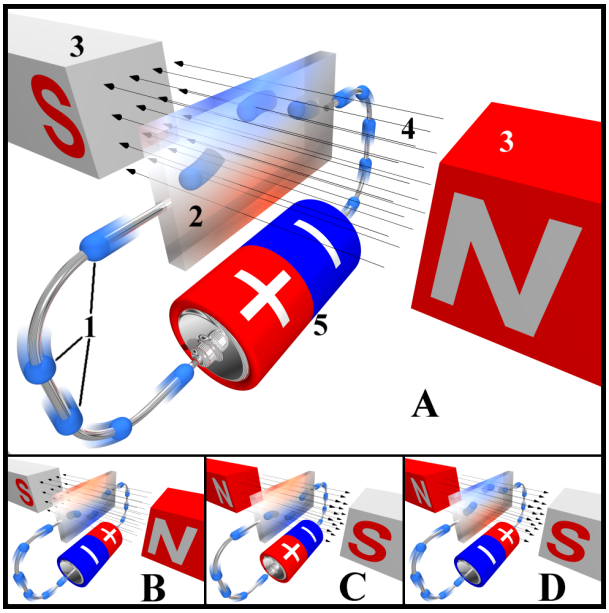


Fig. 24. Artists view of the Hall effect, taken from [15]

surable when a Hall effect sensor is irradiated with protons, but only at higher fluxes. Therefore, the recorded proton test measurements are less affected than the heavy ion test results.

## VII. Conclusion

During the irradiation with protons and up till the end of the irradiation with the Co60 source, no error was measured and the supply current was within the rated limits. Furthermore, we measured no significant differences between the temperature cycled devices and the un-cycled ones. This reflects the results of the performed package analysis by means of X-raying after the thermal cycling test campaign. Thereby, no damage was observed.

The TID test (ELDRS) was stopped after 230 Gy(Si), due to the stiff time frame of the project and limitations due to the Covid pandemic. For MMX it is more than two times of the requested TID tolerance at the component level.

During former test campaigns with a different lot, TID tests and an irradiation with heavy ions were conducted. The TID test was stopped after 1160 Gy(Si) (high dose test) respectively after 520 Gy(Si) (ELDRS test). Similar to the actual test campaign, no serious error was observed. During the irradiation with heavy ions, the output signal was influenced by the particles, but no latch-up was measured. For comparison, some test results of Optek Hall effect sensors could be found at [17].

In summary, the results of the actual test campaign, which is in line with the former test campaigns, make the Infinion Hall effect sensor TLE4945L a promising flight candidate, if minor radiation based deviations in the sensor response to magnetic fields do not pose problems for the application. For missions where a large amount of heavy ions or protons are expected, the tested devices would require further investigation for their suitability.

## VIII. Acknowledgement

This work was performed within the Spacehand and MMX project framework and supported by multiple colleagues of the DLR Institute of Robotics and Mechatronics. The authors would like to thank them for their support.

## References

[1] S. Ulamec, P. Michel, M. Grott *et al.*, "A rover for the JAXA MMX Mission to Phobos," in *70th International Astronautical Congress, Washington DC, 2019*, 2019.

[2] H.-J. Sedlmayr, S. Barthelmes, R. Bayer *et al.*, "MMX - Development of a Rover Locomotion System for Phobos," in *2020 IEEE Aerospace Conference*, 2020.

[3] S. Barthelmes, T. Bahls, R. Bayer *et al.*, "MMX Rover Locomotion Subsystem – Development and Testing towards the Flight Model," in *2022 IEEE Aerospace Conference*, 2022.

[4] H.-J. Sedlmayr, A. Beyer, K. Kunze, and M. Maier, "Radiation test of a BLDC motor driver component," in *2018 IEEE Radiation Effects Data Workshop*, 2018.

[5] Infineon Technologies AG, "TLE4945-2L magnetic bipolar switch with digital output signal," 2022, https://www.infineon.com/cms/de/product/sensor/magnetic-sensors/magnetic-position-sensors/hall-switches/tle4945-2l/.

[6] TT Electronics, OPTEK Technology, "OMH3075 high reliability hallogic hall effect sensor," 2022, https://www.ttelectronics.com/TTElectronics/media/ProductFiles/Datasheets/OMH090-3075.pdf.

[7] M. Newton, H. Wang, L. Chen *et al.*, "Laser single event effects response of optek and infineon hall effect sensors," in *2016 IEEE Radiation Effects Data Workshop*, 2016.

[8] R. Philips, M. Palladino, and C. Camilie, "Development of Brushed and Brushless DC Motors for use in the ExoMars Drilling and Sampling Mechanism," in *41th Aerospace Mechanisms Symposium, Pasadena, 2012*, 2012.

[9] (2022) ((e)xo(m)ars. [Online]. Available: https://de.wikipedia.org/wiki/ExoMars

[10] (2022) SPENVIS - SPace ENVironment Information System. [Online]. Available: https://www.spenvis.oma.be/

[11] (2022) KRP Mechatec GmbH, Garching. [Online]. Available: https://www.krp-m.de/index.php/lang-en/

[12] (2021) Helmholtz Zentrum Berlin Wannsee, Cobalt-60-Source. [Online]. Available: https://www.helmholtz-berlin.de/forschung/oe/be/protonentherapie/index_en.html

[13] N. Meidinger, "Strahlenhärte von röntgen-sperrschicht-ccd-detektoren," Ph.D. dissertation, Technische Universität München, Fakultät für Physik, 2003.

[14] (2021) University of Jyvaskyla, Radiation Effects Facility - RADEF. [Online]. Available: https://www.jyu.fi/science/en/physics/research/infrastructures/accelerator-laboratory/radiation-effects-facility

[15] Wikipedia, en, "Hall effect," 2022, https://en.wikipedia.org/wiki/Hall_effect.

[16] Wikipedia, de, "Hall effect," 2022, https://de.wikipedia.org/wiki/Hall-Effekt.

[17] A. B. Sanders, H. S. Kim, and A. Phan, "Tid and see response of optek hall effect sensors," in *2008 IEEE Radiation Effects Data Workshop*, 2008.